Research Article | Vol. 29, No. 22 / 25 Oct 2021 / Optics Express 36321
Optics EXPRESS

51-W average power, 169-fs pulses from an ultrafast non-collinear optical parametric oscillator

L. LANG,* C. P. BAUER, C. R. PHILLIPS, AND U. KELLER

Institute for Quantum Electronics, ETH Zurich, 8093 Zurich, Switzerland
*langl@phys.ethz.ch

Abstract: We present a high power optical parametric oscillator (OPO) synchronously pumped by the second-harmonic of a modelocked 1030-nm thin-disk laser (TDL) oscillator. The OPO delivers an average power of 51.1 W around degeneracy (1030 nm) with a 10.2-MHz repetition-rate. After extra-cavity dispersion compensation using dispersive mirrors, we obtain a pulse duration of 169 fs, which is 4.6× shorter than the TDL pulse duration of 770 fs. The TDL has 250 W average power, which is converted to 215 W at the second-harmonic. Hence, the OPO exhibits a high photon conversion efficiency of 47% (ratio of signal photons to 515-nm pump photons). Moreover, the OPO generates a peak power of 26.2 MW, which is very similar to the 28.0-MW peak power of the TDL. To facilitate continuous tuning around degeneracy and convenient extraction of the pump and idler beams, the OPO is operated in a noncollinear configuration. A linear cavity configuration was chosen since it offers easy alignment and straightforward cavity length tuning. To the best of our knowledge, this source has the highest average power generated by any ultrafast OPO, and the shortest pulse duration for any >5-W OPO. This result is an important step to adding wavelength tunability to high power Yb-based laser sources without the complexity of either laser or parametric amplifier systems.

1. Introduction

High-power ultrafast sources find numerous applications both in industry and research, such as high-speed and high-precision micromachining, high repetition rate attosecond science, and generating long-wavelength sources via frequency conversion. In many cases, the requirements for these applications can be met with high-power laser oscillators or amplifiers. For some applications however, optical parametric oscillators (OPOs) offer several advantageous features. First, since the gain mechanism is based on a second-order nonlinear process, a wide range of wavelengths is accessible, with the output of the OPO typically being continuously tunable over some wavelength range. And second, the conversion process results in two beams with highly correlated properties but adjustable wavelength difference. Together, these properties make OPOs highly attractive for applications such as frequency conversion, nonlinear spectroscopy methods, pulse compression, and intracavity nonlinear processes. While optical parametric chirped pulse amplification (OPCPA) systems have been power scaled extensively in recent years using Yb-based amplifiers [1], power-scaling of OPOs has not been explored as extensively, despite the potential advantages in terms of system simplicity, beam quality, and efficiency compared with OPCPAs.

To date, the highest average output power demonstrated from an ultrafast OPO is 19 W at 56-MHz repetition rate, corresponding to 0.34-μJ pulses [2]. More recent high-power results achieved less average power, but offer advantages in other parameters, such as rapid tunability [3] or output wavelengths in the UV or towards the mid-IR [4]. Further power scaling of OPOs would benefit many applications, especially where efficiency is limited either by peak or by average power. This includes high harmonic generation (HHG) [5,6], difference-frequency generation

#440189 https://doi.org/10.1364/OE.440189
Journal © 2021 Received 12 Aug 2021; revised 29 Sep 2021; accepted 5 Oct 2021; published 19 Oct 2021

Optics EXPRESS

(DFG) towards the far-infrared and THz spectral regions [7], and electro-optic sampling [8]. Other areas where high power combined with wavelength tunability could be beneficial include multiphoton microscopy [9], Raman spectroscopy [10], and selective material processing [11].

Here, we demonstrate an ultrafast non-collinear high-power OPO with a pump based on a high-power modelocked thin-disk laser (TDL). The TDL has an average power of 250 W at a repetition rate of 10.2 MHz, which we frequency-double to 215 W via second-harmonic generation (SHG). This 515-nm beam is used to synchronously pump a non-collinear OPO with signal and idler tunable around degeneracy (1030 nm). We compress the signal pulses using dispersive mirrors after the output of the OPO, and achieve pulse durations of 169 fs, which is 4.6× shorter than the pulses of the TDL pump. We achieve a signal output power of up to 51.1 W at a repetition rate of 10.2 MHz. This is a 2.5× improvement in average power compared to existing OPOs with sub-picosecond pulses [2]. The pulse energy is 5.0 µJ, the highest pulse energy from any ultrafast OPO, to the best of our knowledge.

2. Experimental setup and results

A frequency doubled high-power ultrafast TDL oscillator is used to pump the OPO. Initially demonstrated by Giesen et. al. in 1994 [12] and first modelocked without Q-switching instabilities in 2000 [13], TDLs offer high average power directly from an ultrafast oscillator with excellent beam quality [14–20], making them an ideal source to drive nonlinear processes with high efficiency. Up to 350 W average power with near-diffraction-limited beam quality have been achieved using a SEmiconductor Saturable Absorber Mirror (SESAM) modelocked TDL [20]. TDLs have been used to pump OPOs in the previous highest-power result [2], and more recently in [21]. In the latter work, the second-harmonic of the TDL was used to non-collinearly pump an OPO operating around degeneracy, similar to our current system discussed here. The TDL used in this work has been previously described in [22], but includes some further optimization of the SESAM to increase the output power from 230 W to 250 W. The laser uses a composite SESAM with a sapphire window bonded to the front side for improved performance, as described in [22]. Compared to [22], the new SESAM has a more favorable cold curvature, and the sapphire window bonded to it is now a-cut instead of c-cut. While both approaches work well, the a-cut configuration should be more robust against stress-induced birefringence at higher powers. The key parameters of this laser are given in Table 1, where they are also compared with the parameters of the OPO.

Table 1. Key parameters of the TDL and of the OPO.

	TDL	OPO
Repetition rate	10.2 MHz	
Average power	250 W	51.1 + 54.6 W (signal + idler)
Center wavelength	1030 nm	1024 nm
Pulse duration	770 fs	169 fs
Spectral bandwidth (FWHM)	1.62 nm	11.6 nm
Time-bandwidth product	1.12×0.315	0.553
Peak power	28.0 MW	26.2 MW
Pulse energy	24.5 µJ	5 µJ
Output coupling rate	30%	21%
Roundtrip GDD	-30600 fs^2	~+1000 fs^2

In the TDL output beam path, we use a 4-axis beam-stabilization system (MRC Systems GmbH). This ensures a stable alignment through the rest of the system even when realigning the

Optics EXPRESS

TDL. The output beam of the TDL is then focused into a 5 mm long low-absorption LiB_3O_5 crystal (LBO, Cristal Laser S.A., absorption specification of <1ppm at 1.07 µm) for type-I SHG (crystal cut: φ=12.8°) using a pair of lenses, as illustrated in Fig. 1(a) (orange path). The crystal is mounted in a passively cooled copper mount with indium foil between the crystal sides and the mount for improved thermal contact. The $1/e^2$ beam radius at the crystal position is around 350 µm, corresponding to a peak intensity of 15 GW/cm^2 when pumping at the full 250 W. We achieve an ultra-high conversion efficiency of more than 85%, with around 215 W of average power at 515 nm. The residual fundamental is separated from the second harmonic using a pair of dichroic mirrors (DM, R>99.95% at 515 ± 5 nm, R<0.5% at 1030 ± 5 nm). The second harmonic is then controlled using a half-wave-plate (HWP, zero-order, EKSMA Optics UAB) and a thin-film polarizer (TFP, Layertec GmbH), allowing for continuous adjustment of the pump power of the OPO. Attenuating the 515-nm pump beam after the SHG crystal ensures that its beam shape and pulse duration do not change when varying the pump power. The OPO cavity (Fig. 1(a), red path) is a linear cavity containing a β-BaB_2O_3 (BBO, CASTECH Inc.) crystal for optical parametric amplification, and a 21% output coupler (OC, Layertec GmbH). The BBO gain crystal is 2 mm long, with the c-axis 27.8° to the surface normal. This configuration is designed for type-I non-collinear phase-matching at 515 nm → 1030 nm + 1030 nm, assuming an external angle between pump and signal of 5°. The crystal is optimized for low absorption (<20 ppm at 1064 nm), and anti-reflective coated for both signal (980-1080 nm, R<0.5%) and pump (515 ± 5 nm, R<1%) on both facets. Similarly to the LBO crystal, the BBO crystal is mounted in a passively cooled copper mount. The polarizations of the interacting beams and the orientation of the crystal is indicated in Fig. 1(a). The pump beam is focused into the crystal using a second pair of lenses, resulting in a $1/e^2$ radius of around 370 µm for the pump beam. This corresponds to a peak intensity of 11 GW/cm^2 when pumping with 215 W. Apart from the BBO crystal and OC, the cavity only contains high-reflective mirrors optimized for high-power ultrashort pulses (Layertec GmbH, R>99.98%, 1000-1100 nm, low-GDD). To avoid excessive nonlinearities on the optics, the cavity mode (Fig. 1(b)) is designed such that its $1/e^2$ radius is >500 µm throughout the cavity. Since the OPO is operated in ambient air, the self-phase modulation (SPM) picked up by the pulses nevertheless has a significant impact on the final pulse shape and spectrum, as we will discuss later. The length of the cavity is matched to the length of the TDL cavity to enable synchronous pumping. Fine tuning of the cavity length is achieved by translating the end mirror using a piezo-actuated translation stage.

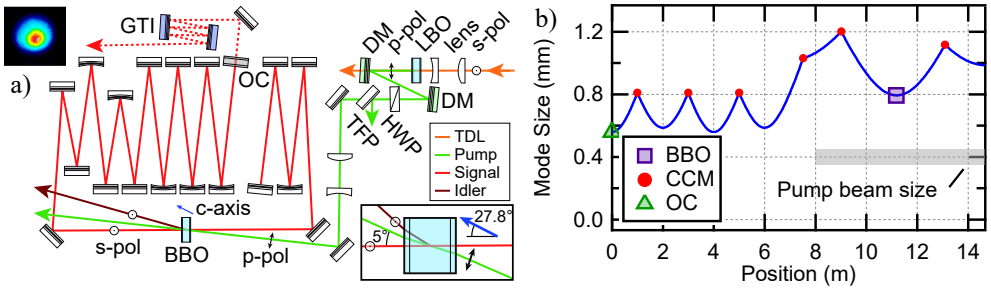

Fig. 1. Design of OPO cavity. a) Layout of the SHG module (orange and green path) and OPO cavity (red path). The polarization of the beams interacting in the two nonlinear crystals is indicated by the arrows, together with the orientation of the c-axis of the BBO crystal. The inset image (top left) shows an image of the cavity mode ($M^2 < 1.1$). The inset diagram (bottom right) shows a close-up of the interaction geometry in the BBO crystal (angles not to scale). b) $1/e^2$ mode size evolution throughout the cavity. The markers indicate the position of the BBO (purple square), the concave mirrors (CCM, red dots) and OC (green triangle), respectively. The gray area indicates the approximate radius of the pump beam at the crystal.

Optics EXPRESS

The roundtrip group-delay-dispersion (GDD) of the cavity is around +1000 fs, resulting from the intracavity air, the BBO crystal, and the residual GDD of the mirrors. The OPO is therefore operating in the positive-dispersion regime, resulting in chirped pulses at the output, as first described in [23]. Outside the OPO cavity, we compress these pulses using a total of 18 bounces on a pair of Gires-Tournois-Interferometer-type dispersive mirrors (GTI) providing -2000 fs^2 per bounce (University of Neuchatel), resulting in a total GDD of -36000 fs^2. The average power and diagnostics are measured after this compression step, to verify that the full power can successfully be compressed.

Next, we present the OPO performance characteristics. For this set of measurements, we set the TDL to its highest output power of 250 W, where it delivers 770-fs pulses with 1.62-nm spectral bandwidth (full-width-at-half-maximum, FWHM). These properties correspond to a time-bandwidth product (TBP) of 0.353, which is 1.12 times the TBP for ideal $sech^2$ pulses (0.315). The orientation of the LBO was readjusted after a short thermalization period of around 10 min to reoptimize the phase matching. The pump power is then scanned by rotating the HWP. At each point, the cavity length is readjusted for optimized output power to compensate for thermally induced repetition rate changes of the TDL. Stable operation is checked by measuring the signal properties with an optical spectrum analyzer (Hewlett Packard), intensity autocorrelator (FEMTOCHROME Research Inc.), and microwave spectrum analyzer (Hewlett Packard). We show the output powers of both signal and idler beam, as well as the optical-to-optical efficiency for the signal beam in Fig. 2(a). As can be seen, we reach up to 51.1 W for the signal and 54.8 W for the idler, corresponding to an optical-to-optical efficiency of 24% (counting only the signal) or 49% (counting both the signal and idler). We believe that this high conversion efficiency is in part due the pump beam being significantly smaller than the cavity mode at the crystal (370 µm compared to 800 µm). This means the pump sees mostly the central part of the signal beam, enabling a homogeneous depletion of the pump. Meanwhile, the large beams result in spatial walk-off being negligible, while the high pulse energies maintain high peak-intensities for efficient conversion even at these larger beam sizes. Finally, we have not noticed any issues due to thermal effects such as thermal lensing or change of the phase matching for the BBO crystal, even at this highest power.

For the point with the highest output power (highlighted in Fig. 2(a)), we characterize the signal pulses using Frequency-resolved Optical Gating (FROG, Femto Easy SAS) [24] to obtain a precise measurement of the pulse duration and shape. The FROG diagnostics are shown in Figs. 2(b)-2(e): Figs. 2(b) and 2(c) show the experimental and retrieved spectrogram, respectively, showing good reconstruction. Figure 2(d) shows the retrieved temporal profile and phase of the pulse, with a temporal FWHM of 169 fs. This corresponds to a compression factor of 4.4× compared to the 0.75-ps pulse duration we have measured without the dispersion compensation installed, and to a 4.6× compression compared to the TDL pulses. Furthermore, the 169-fs pulse duration is very close to transform limited pulse duration of 150 fs. Based on the retrieved temporal profile of the pulses, we compute the peak power of the OPO pulses to be 26.2 MW, which is very similar to the 28.0-MW peak power of the TDL. We therefore achieve wavelength tunability without having to sacrifice peak power. Finally, Fig. 2(e) shows the retrieved spectral profile and phase, with a spectral FWHM of 11.6 nm, corresponding to a TBP of 0.553. For reference, the optical spectrum of the TDL is shown in blue. As can be seen, the output of the OPO is significantly broadened compared to the TDL spectrum. As further cross-check of the retrieved pulse parameters, we also show the optical spectrum of the OPO output as recorded by an optical spectrum analyzer (OSA) in gray. Apart from a slight shift in wavelength, the retrieved spectrum matches the directly measured spectrum, as expected. We attribute this shift to a combination of the drift of the OPO wavelength caused by thermally induced repetition rate changes in the pump TDL, together with the difficulty to synchronize data acquisition of the

Optics EXPRESS

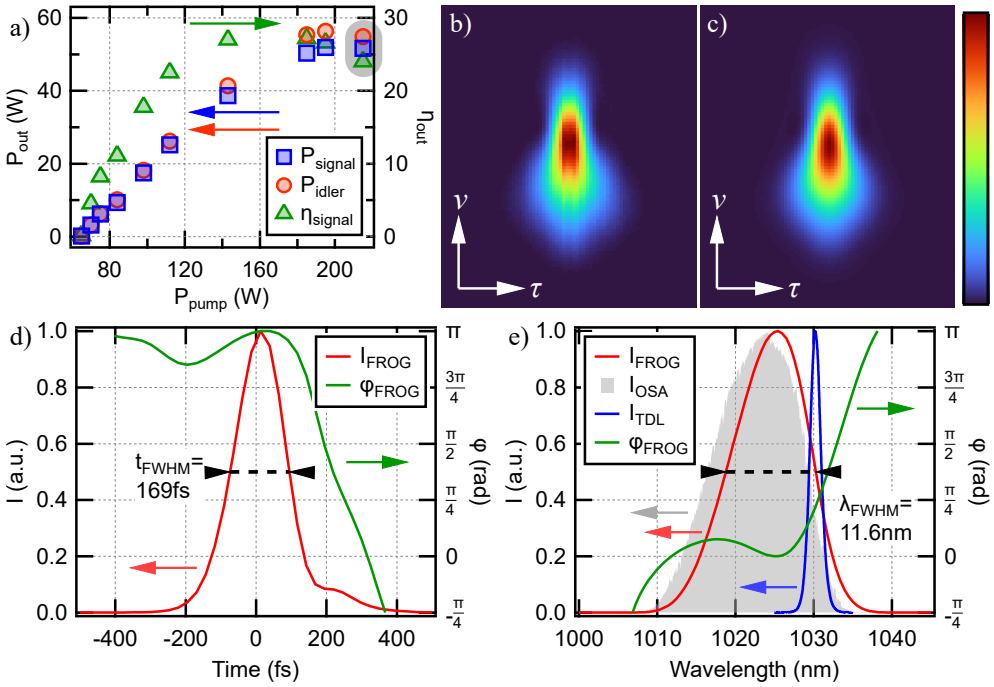

Fig. 2. Diagnostics of the OPO output. a) Output power of the signal (blue squares) and idler (red circles), respectively as a function of pump power. Also shown is the optical-to-optical efficiency of the signal beam (green triangles). b-e) detailed diagnostics at the highest output power (highlighted point in a). b) Measured and c) retrieved FROG spectrogram. d) Temporal shape of the pulses as retrieved from the FROG measurement (red), together with the temporal phase (green). e) Optical spectrum of the OPO pulses, as measured with the OSA (grey) and as retrieved from the FROG measurement (red). Also shown is the spectrum of the TDL (blue), and the spectral phase (green).

FROG and OSA. OPO wavelength drifts could be suppressed by active stabilization of the cavity length [25]. A summary of the key parameters of the OPO is given in Table 1.

As previously noted, the OPO is operating in the positive dispersion regime, leading to the strongly chirped output pulses. The pulse duration of such systems after dispersion compensation is typically limited to around half the duration of the pump pulses [26,27]. In our current work however, we have observed a 4.6× shortening of the pulses. We attribute the comparatively strong compression to a combination of two effects. First, as previously shown in [28], increasing the SPM picked up by the intracavity pulses can lead to broader signal pulses. Due to the high peak powers reached in our OPO, the intracavity air itself is the main source of nonlinearity and provides an estimated B-integral of 0.22 rad, for a total of 0.26 rad per roundtrip. This comparatively large SPM enables strong spectral broadening. Second, signal components that are not temporally overlapped with the pump are rapidly suppressed due to the large OC rate of 21%. This effect prevents the signal pulses from getting significantly longer than the pump pulses. This behavior is in contrast to typical OPOs operating in the positive GDD regime, where the uncompressed signal pulses are significantly longer than the pump pulses.

3. Discussion and conclusions

We demonstrate a high-power non-collinear OPO enabled by a frequency doubled high-power TDL. The system can deliver up to 51.1-W average power with a FWHM pulse duration of 169 fs.

Optics EXPRESS

The output power is 2.5× higher compared to existing ultrafast OPOs, and the pulses are 4.6× shorter than the pulses of the TDL whose second-harmonic pumps the OPO. Combined with the idler at very close wavelengths and similar power levels, this makes this system a promising source for high-power far-infrared and terahertz generation via difference-frequency generation as first demonstrated in [29]. Such schemes typically have very low conversion efficiencies and would thus greatly benefit from high average powers such as the total of 100 W delivered by our system.

Another potential application of such a system is for high-harmonic generation (HHG). Especially at high repetition rates, reaching the pulse energies required for HHG becomes challenging. Suitable sources include Yb-amplifiers or OPCPA systems. They are however either limited to a single wavelength in the case of Yb-amplifiers or highly complex in the case of OPCPAs. Our system achieves a flexible output wavelength while being significantly less complex than OPCPA systems and still delivering 5-µJ pulses. This level of pulse energy is sufficient for directly driving HHG as first demonstrated in [30] for 7-µJ pulses, or more recently in [31] for 1-µJ pulses. High power oscillators are also attractive for driving intracavity nonlinear frequency conversion processes such as HHG [32] and THz generation [33,34]. Compared to passively modelocked oscillators, driving nonlinear processes inside an actively modelocked cavity such as a synchronously pumped OPO may be more robust against modelocking instabilities, and offers wavelength tunability.

Finally, we note the potential to change the wavelength range of the OPO by simply replacing the cavity mirrors and rotating the crystal, enabling high powers also in other wavelength ranges of interest, such as the 800 nm range. Because of the non-collinear pumping configuration, standard broadband optics for Ti:sapphire lasers could be used. Besides providing additional flexibility in implementing the aforementioned frequency generation schemes, this could make the source attractive for even more applications, such as high-speed two-photon imaging using the signal or three-photon imaging using the idler.

Funding. Schweizerischer Nationalfonds zur Förderung der Wissenschaftlichen Forschung (200020_200416).

Acknowledgements. The authors acknowledge support of the technology and cleanroom facility FIRST of ETH Zurich for advanced micro- and nanotechnology. The authors would also like to thank Dr. Valentin Wittwer, and Prof. Dr. Thomas Südmeyer (University of Neuchatel) for providing the dispersive mirrors used in the dispersion compensation setup.

Disclosures. The authors declare no conflicts of interest.

Data availability. Data underlying the results presented in this paper are not publicly available at this time but may be obtained from the authors upon reasonable request.

References

1. K. Mecseki, M. K. R. Windeler, A. Miahnahri, J. S. Robinson, J. M. Fraser, A. R. Fry, and F. Tavella, "High average power 88 W OPCPA system for high-repetition-rate experiments at the LCLS x-ray free-electron laser," Opt. Lett. **44**(5), 1257–1260 (2019).
2. T. Südmeyer, E. Innerhofer, F. Brunner, R. Paschotta, T. Usami, H. Ito, S. Kurimura, K. Kitamura, D. C. Hanna, and U. Keller, "High-power femtosecond fiber-feedback optical parametric oscillator based on periodically poled stoichiometric LiTaO3," Opt. Lett. **29**(10), 1111–1113 (2004).
3. Y. Binhammer, T. Binhammer, R. Mevert, T. Lang, A. Rück, and U. Morgner, "Fast-tunable femtosecond visible radiation via sum-frequency generation from a high power NIR NOPO," Opt. Express **29**(14), 22366–22375 (2021).
4. C. Gu, M. Hu, J. Fan, Y. Song, B. Liu, L. Chai, C. Wang, and D. T. Reid, "High power tunable femtosecond ultraviolet laser source based on an Yb-fiber-laser pumped optical parametric oscillator," Opt. Express **23**(5), 6181–6186 (2015).
5. C. M. Heyl, C. L. Arnold, A. Couairon, and A. L'Huillier, "Introduction to macroscopic power scaling principles for high-order harmonic generation," J. Phys. B: At., Mol. Opt. Phys. **50**(1), 013001 (2017).
6. F. Emaury, A. Diebold, C. J. Saraceno, and U. Keller, "Compact extreme ultraviolet source at megahertz pulse repetition rate with a low-noise ultrafast thin-disk laser oscillator," Optica **2**(11), 980–984 (2015).
7. Y. J. Ding, "Progress in terahertz sources based on difference-frequency generation [Invited]," J. Opt. Soc. Am. B **31**(11), 2696–2711 (2014).
8. A. Weigel, P. Jacob, D. Gröters, T. Buberl, M. Huber, M. Trubetskov, J. Heberle, and I. Pupeza, "Ultra-rapid electro-optic sampling of octave-spanning mid-infrared waveforms," Opt. Express **29**(13), 20747–20764 (2021).

Optics EXPRESS

9. J. Peti-Peterdi, J. L. Burford, and M. J. Hackl, "The first decade of using multiphoton microscopy for high-power kidney imaging," Am. J. Physiology-Renal Physiol. **302**(2), F227–F233 (2012).
10. B. Sophie, F. Patrick, W. Nico, B. Sophie, R. Hervé, B. Cyrille, and D. M. Didier, "Optical parametric oscillator-based light source for coherent Raman scattering microscopy: practical overview," J. Biomed. Opt. **16**(2), 021106 (2011).
11. M. R. Aleksej, G. Mikhail, M. Andrejus, C. Gediminas, and U. Nortautas, "High average power picosecond laser for selective material processing at 1342 nm wavelength," Proc. SPIE **9342**, 93421J (2015).
12. A. Giesen, H. Hugel, A. Voss, K. Wittig, U. Brauch, and H. Opower, "Scalable Concept for Diode-Pumped High-Power Solid-State Lasers," Appl. Phys. B **58**(5), 365–372 (1994).
13. J. Aus der Au, G. J. Spühler, T. Südmeyer, R. Paschotta, R. Hövel, M. Moser, S. Erhard, M. Karszewski, A. Giesen, and U. Keller, "16.2 W average power from a diode-pumped femtosecond Yb:YAG thin disk laser," Opt. Lett. **25**(11), 859–861 (2000).
14. C. J. Saraceno, F. Emaury, O. H. Heckl, C. R. E. Baer, M. Hoffmann, C. Schriber, M. Golling, T. Südmeyer, and U. Keller, "275 W average output power from a femtosecond thin disk oscillator operated in a vacuum environment," Opt. Express **20**(21), 23535–23541 (2012).
15. C. J. Saraceno, F. Emaury, C. Schriber, M. Hoffmann, M. Golling, T. Südmeyer, and U. Keller, "Ultrafast thin-disk laser with 80 µJ pulse energy and 242 W of average power," Opt. Lett. **39**(1), 9–12 (2014).
16. J. Brons, V. Pervak, E. Fedulova, D. Bauer, D. Sutter, V. Kalashnikov, A. Apolonskiy, O. Pronin, and F. Krausz, "Energy scaling of Kerr-lens mode-locked thin-disk oscillators," Opt. Lett. **39**(22), 6442–6445 (2014).
17. J. Brons, V. Pervak, D. Bauer, D. Sutter, O. Pronin, and F. Krausz, "Powerful 100-fs-scale Kerr-lens mode-locked thin-disk oscillator," Opt. Lett. **41**(15), 3567–3570 (2016).
18. J. Zhang, K. F. Mak, and O. Pronin, "Kerr-Lens Mode-Locked 2-µm Thin-Disk Lasers," IEEE J. Sel. Top. Quantum Electron. **24**, 1–11 (2018).
19. N. Modsching, J. Drs, J. Fischer, C. Paradis, F. Labaye, M. Gaponenko, C. Kränkel, V. J. Wittwer, and T. Südmeyer, "Sub-100-fs Kerr lens mode-locked Yb:Lu2O3 thin-disk laser oscillator operating at 21 W average power," Opt. Express **27**(11), 16111–16120 (2019).
20. F. Saltarelli, I. J. Graumann, L. Lang, D. Bauer, C. R. Phillips, and U. Keller, "Power scaling of ultrafast oscillators: 350-W average-power sub-picosecond thin-disk laser," Opt. Express **27**(22), 31465–31474 (2019).
21. T. Lang, T. Binhammer, S. Rausch, G. Palmer, M. Emons, M. Schultze, A. Harth, and U. Morgner, "High power ultra-widely tuneable femtosecond pulses from a non-collinear optical parametric oscillator (NOPO)," Opt. Express **20**(2), 912–917 (2012).
22. L. Lang, F. Saltarelli, G. Lacaille, S. Rowan, J. Hough, I. J. Graumann, C. R. Phillips, and U. Keller, "Silicate bonding of sapphire to SESAMs: adjustable thermal lensing for high-power lasers," Opt. Express **29**(12), 18059–18069 (2021).
23. D. C. Edelstein, E. S. Wachman, and C. L. Tang, "Broadly tunable high repetition rate femtosecond optical parametric oscillator," Appl. Phys. Lett. **54**(18), 1728–1730 (1989).
24. D. J. Kane and R. Trebino, "Characterization of Arbitrary Femtosecond Pulses Using Frequency-Resolved Optical Gating," IEEE J. Quantum Electron. **29**(2), 571–579 (1993).
25. J. Chesnoy and L. Fini, "Stabilization of a femtosecond dye laser synchronously pumped by a frequency-doubled mode-locked YAG laser," Opt. Lett. **11**(10), 635–637 (1986).
26. J. M. Dudley, D. T. Reid, M. Ebrahimzadeh, and W. Sibbett, "Characteristics of a noncritically phasematched Ti:sapphire pumped femtosecond optical parametric oscillator," Opt. Commun. **104**(4-6), 419–430 (1994).
27. Q. Fu, G. Mak, and H. M. van Driel, "High-power, 62-fs infrared optical parametric oscillator synchronously pumped by a 76-MHz Ti:sapphire laser," Opt. Lett. **17**(14), 1006 (1992).
28. P. Liu and Z. Zhang, "Chirped-pulse optical parametric oscillators," Opt. Lett. **43**(19), 4735–4738 (2018).
29. F. Zernike and P. R. Berman, "Generation of Far Infrared as a Difference Frequency," Phys. Rev. Lett. **15**(26), 999–1001 (1965).
30. F. Lindner, W. Stremme, M. G. Schätzel, F. Grasbon, G. G. Paulus, H. Walther, R. Hartmann, and L. Strüder, "High-order harmonic generation at a repetition rate of 100 kHz," Phys. Rev. A **68**(1), 013814 (2003).
31. A. Vernaleken, J. Weitenberg, T. Sartorius, P. Russbueldt, W. Schneider, S. L. Stebbings, M. F. Kling, P. Hommelhoff, H. D. Hoffmann, R. Poprawe, F. Krausz, T. W. Hansch, and T. Udem, "Single-pass high-harmonic generation at 20.8 MHz repetition rate," Opt. Lett. **36**(17), 3428–3430 (2011).
32. F. Labaye, M. Gaponenko, N. Modsching, P. Brochard, C. Paradis, S. Schilt, V. J. Wittwer, and T. Südmeyer, "XUV Sources Based on Intra-Oscillator High Harmonic Generation With Thin-Disk Lasers: Current Status and Prospects," IEEE J. Sel. Top. Quantum Electron. **25**(4), 1–19 (2019).
33. J. E. Schaar, K. L. Vodopyanov, P. S. Kuo, M. M. Fejer, X. Yu, A. Lin, J. S. Harris, D. Bliss, C. Lynch, V. G. Kozlov, and W. Hurlbut, "Terahertz Sources Based on Intracavity Parametric Down-Conversion in Quasi-Phase-Matched Gallium Arsenide," IEEE J. Sel. Top. Quantum Electron. **14**(2), 354–362 (2008).
34. M. Hamrouni, J. Drs, N. Modsching, V. J. Wittwer, F. Labaye, and T. Südmeyer, "Intra-oscillator broadband THz generation in a compact ultrafast diode-pumped solid-state laser," Opt. Express **29**(15), 23729–23735 (2021).